An Effective Two-stage Noise Training Methodology for Classification of Breast Ultrasound Images

Yiming Bian[a] and Arun K. Somani[b]

Department of Electrical and Computer Engineering, Iowa State University, Ames, Iowa, U.S.A.

Keywords: Noise Training, Single-noise Training, Mix-noise Training, Breast Ultrasound Image, Image Classification.

Abstract: Breast cancer is one of the most common and deadly diseases. An early diagnosis is critical and in-time treatment can help prevent the further spread of cancer. Breast ultrasound images are widely used for diagnosis, but the diagnosis heavily depends on the radiologist's expertise and experience. Therefore, computer-aided diagnosis (CAD) systems are developed to provide an effective, objective, and reliable understanding of medical images for radiologists and diagnosticians. With the help of modern convolutional neural networks (CNNs), the accuracy and efficiency of CAD systems are greatly improved. CNN-based methods rely on training with a large amount of high-quality data to extract the key features and achieve a good performance. However, such noise-free medical data in high volume are not easily accessible. To address the data limitation, we propose a novel two-stage noise training methodology that effectively improves the performance of breast ultrasound image classification with speckle noise. The proposed mix-noise-trained model in Stage II trains on a mix of noisy images at multiple different intensity levels. Our experiments demonstrate that all tested CNN models obtain resilience to speckle noise and achieve excellent performance gain if the mix proportion is selected appropriately. We believe this study will benefit more people with a faster and more reliable diagnosis.

1 INTRODUCTION

Breast cancer is one of the most deadly diseases for people, especially women, all around the world. Currently, ultrasound scanning is widely adopted as a complimentary diagnose method. However, the diagnosis heavily depends on the experience of the radiologist, which may be slow, expensive, and sometimes not as accurate for everyone. For better ultrasound image understanding, CAD systems are developed using machine learning algorithms. It also helps to overcome the shortcomings of ultrasound diagnosis and helps doctors improve the accuracy and efficiency of diagnosis (Wang et al., 2021). The use of ultrasound-based CAD for the classification of tumor diseases provided an effective decision-making support and a second tool option for radiologists or diagnosticians (Liu et al., 2019).

CNN-based studies have pushed great progresses in medical image classification field. Most backbone CNN architectures were proposed with the development of ImageNet Large Scale Visual Recognition Challenge (ILSVRC) (Russakovsky et al., 2015). In 2009, a large database, which contains over 14 million hand-annotated images, designed for visual object recognition research called ImageNet was presented by Li Fei-Fei et al. (Deng et al., 2009). In the follwoing year, ImageNet project began an annual contest called ILSVRC. This challenge uses a subset of ImageNet that has $1,000$ non-overlapping classes of objects. As it is commonly acknowledged that the average recognition capability of human has a top-5 error rate of 5%, the winner in 2015, *ResNet* (He et al., 2016), beat human-level object recognition capability for the first time with a top-5 error rate of 3.6%. The state-of-the-art model, *Florence* (Yuan et al., 2021), achieved an extraordinary top-5 error rate of 0.98%. As the annual champion models having a deeper and deeper architecture, deep neural networks have proved to be practical and effective in image classification tasks. All of these intriguing figures and achievements indicate that the improvement of classification accuracy on high-quality images is not a big challenge anymore.

However, image classification in medical areas still faces great difficulties. The shortage of large volume of high-quality medical data is an undeniable

[a] https://orcid.org/0000-0002-8725-3603
[b] https://orcid.org/0000-0002-6248-4376

Bian, Y. and Somani, A.
An Effective Two-stage Noise Training Methodology for Classification of Breast Ultrasound Images.
DOI: 10.5220/0011553000003335
In *Proceedings of the 14th International Joint Conference on Knowledge Discovery, Knowledge Engineering and Knowledge Management (IC3K 2022) - Volume 1: KDIR*, pages 83-94
ISBN: 978-989-758-614-9; ISSN: 2184-3228

predicament. Ultrasound medical datasets are more difficult to obtain as the annotation of medical images requires significant professional medical knowledge (Liu et al., 2019). Moreover, most patients prefer to keep their health data private, which makes public medical data a very rare resource. Another obstacle is the medical data acquisition device difference. Not all devices produce high-quality images that reflect key features of the target object. Also, the complexity nature of disease itself, such as massive amount of contour patterns of a malignant tumor, prevents the medical image annotation from totally reliable and poses great challenges for a CNN model to generalize.

Given the fact that most medical data, including ultrasound images, inevitably contain speckle noise during the acquisition process. Noisy data is another significant obstacle for CNN-based studies. After years of studies, researchers have developed effective despeckling techniques that improve the performance of CNN models.

1.1 Related Work

Previous researchers have accomplished great outcomes on speckle noise suppression while keeping the edge information and preserving a high-quality contour in breast ultrasound images. In (Bhateja et al., 2014), Bhateja, Vikrant, et al. present a modified speckle suppression algorithm using directional average filters for breast ultrasound images in homogeneity domain. Their simulation results show significant performance improvement regarding speckle noise removal and edge preservation. In (Virmani et al., 2019), Virmani, Jitendra, and Ravinder Agarwal propose a detail preserving anisotropic diffusion (DPAD) despecking filtering algorithm that optimally reduces the speckle noise from ultrasound images by retaining texture information and enhancing the tumor edges. In (Chang et al., 2019), Chang, Yi, et al. remove the noise in medical images from image decomposition perspective. They treat the noise and image components equally and propose a two-stage CNN that models both the image and noise simultaneously. In (Li et al., 2022), Li, Xiaofeng, et al. propose a fast speckle noise suppression algorithm in breast ultrasound image using three-dimensional deep learning. Their experiment results demonstrate that the speckle noise suppression time is low, the edge information is well preserved and the image details are visible.

CNN-based methods were adopted for medical image understanding. In (Liu et al., 2019), Liu, Shengfeng, et al. review popular deep learning architectures and thoroughly discuss their applications in ultrasound image analysis such as classification, detection and segmentation. In (Sarvamangala and Kulkarni, 2021), Sarvamangala, D. R., and Raghavendra V. Kulkarni provide a comprehensive survey of applications of CNNs in medical image understanding such as X-ray, magnetic resonance imaging (MRI), computed tomography (CT) and ultrasound scanning. In (Daoud et al., 2019), Daoud, Mohammad I., Samir Abdel-Rahman, and Rami Alazrai investigate the use of deep features extraction and transfer learning to enable the use of a pretrained CNN model to achieve accurate classification of breast ultrasound images. Their results suggest that an accurate breast ultrasound image classification can be achieved with features extracted from the pretrained CNN model and effective feature selection algorithms.

Medical data scarcity problem is one of the greatest obstacles in CNN-related researches. To mitigate this issue, transfer learning has been adopted in majority of related studies. In (Kim et al., 2022), Kim, Hee E., et al. provide actionable insights on how to select backbone CNN models and tune them with consideration of medical data characteristics. For example, they suggest that the model should be fine-tuned by incrementally unfreezing convolutional layers from top to bottom layers with a low learning rate. In (Ayana et al., 2022), Ayana, Gelan, et al. propose a multistage transfer learning algorithm and their results show the significant improvement in the classification performance of breast ultrasound images. In (Wang et al., 2021), Wang, Yu, et al. review the data preprocessing methods of medical ultrasound images, including data augmentation, denoising and enhancement. They explicitly mentioned that traditional machine learning methods are vulnerable to possible low imaging quality and deep learning can reduce this impact by extracting high-level features.

1.2 Contributions

In this work, we focus on improving the performance of CNN models on classifying breast ultrasound images with speckle noise. We explore the impact of noisy data training on noisy data classification. Facing the data shortage problem during our experiments, we mitigate this issue and overcome class imbalance problem by applying augmentation and oversampling techniques. Finally, we propose a systematic two-stage noise training methodology that improves the classification performance of the selected CNN architectures on noisy data. Tested models show excellent resilience to speckle noise after applying our methodology. We also provide empirical parameter choices for generating ultrasound images with artificial noise, constructing noisy datasets, training networks and obtain the model with the best performance.

The rest of the paper is organized as follows. Section II provides preliminary knowledge of speckle noise, deep convolutional networks and image classification. Our two-stage noise training methodology is introduced in Section III. Section IV describes how all the datasets are prepared and how the corresponding CNN models are developed. We present our experiments, results and detailed analysis in Section V. Conclusions and future research directions are discussed in Section VI.

2 BACKGROUND

In this section, we provide prerequisite knowledge of speckle noise, deep neural networks and image classification. Specifically, we answer the following questions: 1) how speckle noise is formed; 2) why speckle noise is common in medical images; 3) how speckle noise is simulated; 4) why deep neural networks are effective on noise medical image processing; and 5) what popular neural network architectures are in medical image classification field.

2.1 Speckle Noise

Speckle is a common phenomenon in images obtained by coherent imaging systems such as synthetic-aperture radar (SAR) and ultrasound machines because the object surface is rough on the scale of wavelength. The reflectivity function of the image acquisition device produces scatterers. These scattered signals add coherently, which forms the patterns of constructive and destructive interference shown as bright and dark dots in the image (Forouzanfar and Abrishami-Moghaddam, 2011). In medical images, especially ultrasound images, speckle noise is almost inevitable because mainstream ultrasound machines are coherent imaging systems, and human tissue and lesion tissue have a rough surface. Fig. 1 shows an SAR image of San Francisco, California and a breast ultrasound image of a benign tumor. Speckle noise in both images can be easily observed.

In our experiments, we simulate speckle noise using "imnoise()" function in MATLAB. This function adds various synthetic noise to the input image. The full documentation is available online by MathWorks

[1] https://www.jpl.nasa.gov/images/pia01751-space-radar-image-of-san-francisco-california

[2] https://www.kaggle.com/datasets/aryashah2k/breast-ultrasound-images-dataset

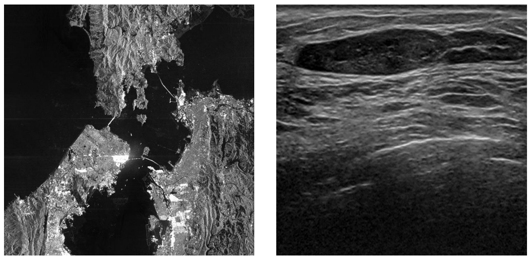

(a) (b)

Figure 1: **(a)** A Space Radar Image of San Francisco, California (Cropped): It was acquired by the Spaceborne Imaging Radar-C and X-Band Synthetic Aperture Radar (SIR-C/X-SAR) aboard space shuttle Endeavour on orbit 56 on October 3, 1994. It is available online by NASA/JPL-Caltech[1]. **(b)** A Breast Ultrasound Image of a Benign Tumor (Cropped): This image is included in a public dataset called Breast Ultrasound Image Dataset (BUSI) (Al-Dhabyani et al., 2020). It is stored under the folder 'BUS/benign' with a filename of '000087'. The whole dataset is available online by Kaggle[2].

Help Center[3]. Speckle noise is multiplicative and it is generated using Equation 1, where the input image (I_{img}) is a matrix of integer numbers, each ranging from 0 to 255. Gray-scale images and RGB images have a third dimension of 1 and 3 respectively. The multiplication is element-wise and the synthetic noise (η) is uniformly distributed with mean (μ) equals to 0 and variance (σ^2) to be specified. The variance, σ^2, controls the intensity of noise. The output image (O_{img}) shares the same dimension with the input image (I_{img}).

$$O_{\text{img}} = I_{\text{img}} + \eta\, I_{\text{img}} \tag{1}$$

The value of an output pixel (o_{pixel}) is determined by σ^2 and the input pixel value (i_{pixel}). Their quantitative relationship is given in Equation 2. The range of o_{pixel} is from 0 to 255. When o_{pixel} is out of the range, it is automatically bounded to the nearest marginal value, thus either 0 or 255.

$$o_{\text{pixel}} = i_{\text{pixel}} + \sqrt{12\sigma^2} \times i_{\text{pixel}} \times [\text{rand}(0,1) - 0.5] \tag{2}$$

As the synthetic noise (η) is uniformly distributed, thus $\eta \sim \mathcal{U}(a,b)$, where a and b are the minimum and maximum values of η. The mean (μ) and variance (σ^2) can be expressed using a and b as given in Equation 3. Then we have $\sqrt{12\sigma^2} = 2b - 2\mu$. Since $\mu = 0$, it is simplified to $\sqrt{12\sigma^2} = 2b$. The range $[a,b]$ can be expressed as $2bm$, where m is a random value and $m \in [-0.5, 0.5]$. The expression $2bm$ can be written as $\sqrt{12\sigma^2} \times [\text{rand}(0,1) - 0.5]$, which explains the multiplication part of Equation 2.

[3] https://www.mathworks.com/help/images/ref/imnoise

$$\begin{cases}\mu = \frac{1}{2}(a+b) \\ \sigma^2 = \frac{1}{12}(b-a)^2\end{cases} \tag{3}$$

Depending on the source of ultrasound images, some are stored as gray-scale while other are RGB images, although they all appear to be gray-scaled. It causes issues in both adding artificial noise and processing using CNN models. Adding speckle noise to an RGB ultrasound image generates noise pixels with colors, which degrades the simulation quality. Therefore, it is necessary to convert the RGB image to gray-scale. On the other hand, the vast majority of CNN models take an RGB image as input. We address both problems by first converting RGB images to gray-scale and add artificial speckle noise. Then we duplicate two more channels and form them into the proper size that is compatible to a CNN's input.

2.2 Deep Neural Networks and Image Classification

A concise introduction to deep neural network has been provided in (Dodge and Karam, 2016). The big picture of deep learning, convolutional neural network, image understanding with deep convolutional networks were discussed in (LeCun et al., 2015). A large amount of research has been done on applying deep neural network to image classification tasks such as aforementioned models in ILSVRC. All of them were trained on a subset of ImageNet, which contains 1,000 non-overlapping classes and has over 1.2 million sample images.

In medical area, however, the lack of large volume of high-quality data poses great challenges. As introduced above, images with noise are common in medical area during the acquisition process. Apart from noise suppression techniques, machine-learning-based methods are gaining more popularity in recent years. Traditional neural networks are vulnerable to low quality images. To address this issue, neural networks with deeper levels are developed as they can extract high-level features and improve the classification performance.

In medical image processing area, some popular backbone CNNs are well-experimented and explored. For example, AlexNet is the main focus in (Nawaz et al., 2018) (Masud et al., 2021). ResNet is studied in (Jiang et al., 2019) (Al-Haija and Adebanjo, 2020) (Virmani et al., 2020) (Yap et al., 2020) (Yu et al., 2020) and VGG16 provides the best performance in (Moon et al., 2020) (Hadad et al., 2017) (Jahangeer and Rajkumar, 2021) (Albashish et al., 2021) (Jahangeer and Rajkumar, 2021).

3 METHODOLOGY

We propose a two-stage noise training methodology as shown in Fig. 2. It improves the robustness of a CNN model regarding noise resilience when processing jobs such as image classification. Two stages are Stage I: single-noise training and Stage II: mix-noise training, or single training and mix training for simplicity. In Stage I, we first construct n noisy sets by adding n levels of noise to the original training data and obtain $n+1$ sets for training purpose. Then we train the CNN model on each set and derive $n+1$ retrained models including one trained on original data and n single-noise-trained, or single-trained models. In Stage II, we mix all $n+1$ training sets at a proportion of (a_0%, a_1%, ..., a_n%), where $\sum_{i=0}^{n} a_i = 100$. Then, we train the CNN model on mix training sets with different proportions. The mix-noise-trained, or mix-trained model with the best performance is selected as the final outcome of our methodology.

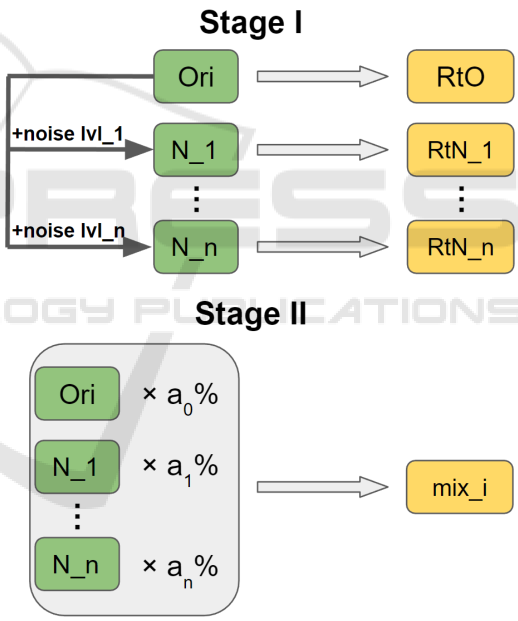

Figure 2: Two-stage noise training methodology: Training sets and models are denoted using green and yellow chunks respectively. "Ori/N_x" stands for a training set that contains original/level-x noisy data. "RtO" stands for a model that is **Ret**rained on **O**ri. "RtN_x" stands for a model that is **Ret**rained on **N_x**. "mix_i" is a mix-trained model.

Here, we provide some empirical selections of aforementioned parameters in the two-stage noise training methodology. Generating noisy data is one of the most significant steps as all the noise-trained models rely on it. The selections for synthetic noise range and granularity are critical. Intuitively, the lower bound of noise level is 0, thus noise-free or the original high-quality image. The upper bound should not be the maximum value of the parameters in the noise-generating function because an image is barely informative or useful when the noise is extremely intense. In ultrasound imaging scenario, an ultrasound machine will be recognized as a failure if it produces noise-dominating ultrasound images. Fixing the machine would be the top priority instead of digging information from barely informative images.

We add speckle noise using "imnoise()" in MATLAB. This function is widely used to generate an artificial noisy image in academic area. The noise intensity is determined by the specified variance. In our experience, 0.1 is a reasonable upper bound and 0.02 is an appropriate step size. If the granularity is finer, there is not much difference between two consecutive noise levels, which introduces redundant information when doing comparison and analysis. In our experiment, we set the range of speckle noise variance to be $[0, 0.1]$ at a step size of 0.02, thus five noisy sets are generated based on the original set.

As there are six models in Stage I, we pick the top three based on the performance on test sets. An all-round comparison can be designed depending on the specific requirements. For example, if the future images are expected to be less noisy, the model's classification performance on sparsely noisy images should be stressed during the comparison process. Then we mix the corresponding training sets at multiple proportion combinations. Tested proportion choices are $(20\%, 40\%, 40\%)$, $(25\%, 50\%, 25\%)$, $(33\%, 33\%, 33\%)$ and $(40\%, 40\%, 20\%)$. The proportion of the rest uncollected sets is 0%, hence is omitted for simplicity. The best mix-trained model will be selected as the final output of this methodology after comprehensive comparisons.

4 DATASETS AND CNN MODELS

4.1 Dataset Preparation

In our experiments, we mainly work on two public breast ultrasound image datasets: Breast Ultrasound Images Dataset (BUSI) (Al-Dhabyani et al., 2020) and MT_small (Badawy et al., 2021). BUSI includes breast ultrasound images among women between 25 and 75 years old. All images were acquired using LOGIQ E9 ultrasound and LOGIQ E9 Agile ultrasound system by Baheya Hospital, Cairo, Egypt in 2018. It has three classes: benign, malignant and normal. The sample size of each class is 487, 210 and 133. MT_small is a modest dataset that contains 200 images for each class of benign and malignant breast cancer ultrasound images.

We drop the samples of normal class in BUSI as the main purpose of the experiments is to determine whether the nodule is benign or malignant. We assume the presence of a nodule. Moreover, we trim both datasets by removing samples with on-image segmentation squares and annotations. This ensures the training data do not have uncommon features that distract the model from convergence. Finally, the trimmed BUSI contains 335 benign and 184 malignant sample images, and the trimmed MT_small contains 187 benign and 179 malignant sample images.

The arrangement details of two datasets are provided in Table 1. BUSI is selected for training purpose because it contains more sample images. As the malignant sample size (184) is much smaller than benign sample size (335), it affects both convergence during the training phase and generalization of a model on the test set (Buda et al., 2018).

In binary classification scenario, class imbalance problem is more detrimental and the output may always be the majority class. To address this issue, undersampling and oversampling are two common measures. Oversampling is widely used and proven to be robust as mentioned in (Ling and Li, 1998). It is also justified that oversampling outperforms all other tested measures with respect to multi-class receiver operating characteristic curve (ROC AUC) in (Buda et al., 2018). Moreover, since both the majority and minority class sample sizes are very small, oversampling is preferred.

It is mentioned in (Buda et al., 2018) that simply replicates randomly selected samples in the minor class is an effective oversampling method. But it may lead to overfitting. Therefore, we randomly select sample images in malignant class and crop them as new samples to avoid potential overfitting issue. The region of interest is ensured to be present in new sample images. Moreover, a validation set that contains no oversampling samples is carefully constructed to mitigate the overfitting risk.

Reasons why other data augmentation methods are not adopted are 1) they are equivalent or similar to cropping; and 2) they do not simulate a properly acquired ultrasound image. For example, as the preprocessing before feeding the image to a CNN formats the input image into the same shape, scaling and translation are very similar to cropping. Rotation and flipping may not simulate a proper ultrasound image because patients are always required to keep an upright position when taking the ultrasound image. Brightness and saturation change may indicate a technical issue with the ultrasound transducer probe. Therefore, we adopt cropping as the augmentation method here. Two classes have the same size

(335) after oversampling. They are further divided into a training set and a validation set at the proportion of 80% and 20% respectively. It is ensured that the dataset for validation does not contain any oversampling samples.

Based on the balanced original dataset, we add five levels of speckle noise using "imnoise()" in MATLAB. The noise variance is set to 0.02, 0.04, 0.06, 0.08 and 0.1 for the single-noise-training process in Stage I. These five BUSI dataset noisy variants are named as *BUSI_SPE_002*, *BUSI_SPE_004* etc. Without causing a confusion, "*BUSI_*" is omitted for simplicity. To determine the best three single-trained models, we compare their classification performance on test sets. Due to the lack of public breast ultrasound image data, we take the whole trimmed BUSI as a test set, together with the trimmed MT_small.

This is a very controversial data usage choice because high similarity between training and test sets enables models to be more optimal than they really are. However, the main focus of this work is to explore the potential performance gain by applying the proposed two-stage noise training methodology. The effectiveness of the proposed methodology can be justified if the over-optimal noise-trained models outperform the over-optimal normally trained models, based on the fact that all of these models are trained and tested on the same datasets or their noisy variants. In addition, extreme medical data shortage is undeniable and cannot be easily solved in the near future. This decision on data usage is hard and choiceless. Each of the two test sets, BUSI and MT_small, also has five noisy variants by adding five levels of speckle noise.

To decrease the shortcoming of this data usage, we comprehensively compare the performance on two test sets. When they conflict, the test performance on MT_small plays a more important role in model ranking. With three Stage I winners, we construct Stage II training and validation sets from single-noise sets in Stage I with multiple mix proportion options: $(20\%, 40\%, 40\%)$, $(25\%, 50\%, 25\%)$, $(33\%, 33\%, 33\%)$ and $(40\%, 40\%, 20\%)$. These four mixed variant datasets are named as *SPE_204040*, *SPE_255025* etc. The order of the corresponding single-noise set is randomly decided because it is often the case that no model is strictly better than another. In our experiment, the corresponding single-noise sets are in the ascending noise intensity order. The same test sets are used to analyze the performance of mix-trained models on images at each noise intensity level.

In conclusion, there are six Stage I training/validation sets, four Stage II train/validation sets and twelve test sets for both stages.

Table 1: Details of all the datasets: The values of i are $\{1, 2\}$ as there are two stages. Two groups of set names are: Group 1: {*Original, SPE_002, SPE_004, SPE_006, SPE_008, SPE_010*}, Group 2: {*SPE_204040, SPE_255025, SPE_333333, SPE_404020*}. B and M in "Sample Size" stand for benign and malignant respectively.

Purpose	**Initial Dataset**	**Dataset Name**	**Sample Size**
Stage_*i* Train	BUSI	Group *i*	B: 268
			M: 268
Stage_*i* Val			B: 67
			M: 67
Test	BUSI	Group 1	B: 335
			M: 184
	MT_small		B: 187
			M: 179

4.2 CNN Models

Previous researchers have done ample experiments on breast ultrasound image classification with CNNs. Several of them are proved to be very effective and used as foundations for further studies. They include AlexNet (Krizhevsky et al., 2012), ResNet (He et al., 2016) and VGG (Simonyan and Zisserman, 2014). Therefore, we select four CNN models in our experiment. They are AlexNet, ResNet-18, ResNet-50 and VGG16. As the pretrained models were trained on ImageNet (Deng et al., 2009), we replace the output dimension of the last fully-connected layer from $1,000$ to 2 for transfer learning in our methodology.

Since the sample size of our whole training set (536) is far from comparable to that of ImageNet ($\geq$ 1.2 million) and medical images are not stressed in ImageNet, feature extraction of our training data could be a huge obstacle. Ayana, Gelan, et al. proposed a multistage transfer learning strategy in (Ayana et al., 2022) that first fine tunes the pretrained model with large amount of cancer cell line images, which can be easily acquired. Then they fine tune the intermediate model with limited-amount breast cancer images to overcome the training data shortage issue and improve the classification performance. We overlook the shortage issue for now as the main purpose of this work is to show the performance improvement brought by noise training even with very limited amount of training data.

All the retrained models during our two-stage noise training methodology are listed in Table 2. In Stage I, six retrained models, including one trained on original data and five single-trained models, are generated by fine tuning the pretrained model. Four mix-trained models in Stage II are also fine-tuned based on the pretrained model and trained on mix datasets.

Table 2: The values of *x* are {*002, 004, 006, 008, 010*}. The values of *y* are {*204040, 255025, 333333, 404020*}.

Stage	CNN	Training Set	Model
I	AlexNet ResNet-18/50 VGG16	*Original*	*RtO*
		SPE_x	*RtN_x*
II		*SPE_y*	*mix_y*

5 EXPERIMENTS AND RESULTS

In this section, we discuss the performance metrics to rank models and briefly introduce the implementation in each stage. The source code of our experiments is public through GitHub[4] for other researchers to reproduce the results and carry out further studies. We also provide detailed model ranking comments and performance analysis of highlighted models in this section.

5.1 Performance Metrics

The performance metrics used in this study are accuracy, specificity, sensitivity and F1 score. True/False indicates the nodule is cancerous/non-cancerous. In the following equations, TP/TN and FP/FN stand for true positive/negative and false positive/negative.

Accuracy given by Equation 4 is the proportion of correct predictions over all types of predictions.

$$Accuracy(\%) = \frac{TP+TN}{TP+TN+FP+FN} \tag{4}$$

Specificity given by Equation 5 is the proportion of predictions that if a nodule is benign, it is classified as false.

$$Specificity(\%) = \frac{TN}{TN+FP} \tag{5}$$

Sensitivity given by Equation 6 is the proportion of predictions that if a nodule is malignant, it is classified as true.

$$Sensitivity(\%) = \frac{TP}{TP+FN} \tag{6}$$

F1 score given by Equation 7 is the harmonic mean of precision and recall (Taha and Hanbury, 2015). Recall is equivalent to sensitivity and precision is defined as $\frac{TP}{TP+FP}$. It describes the reliability of a positive prediction.

$$F1(\%) = \frac{TP}{TP+\frac{1}{2}(FP+FN)} \tag{7}$$

Among all four measurements, we rank the priority as sensitivity, F1 score, accuracy and specificity. When a nodule is benign but tested otherwise, the patient could have a second check if the classification is wrong. The probability of multiple consecutive wrong classification is significantly low. On the contrary, if the nodule is malignant and the result shows different, it is fatal because it does not raise attention. We view it as the most critical principle that if a nodule is malignant, the model outputs true, thus TP and FN are more emphasized. Therefore, sensitivity is the most significant while specificity is the least.

[4]https://github.com/YimingBian/Speckle_noise_IC

5.2 Stage I

In Stage I, we fine tune the pretrained model on six training sets. We obtain *RtO* and five single-trained *RtN* models. We then analyze their performance in four aspects based on the test results on both BUSI and MT_small test sets. Here are two basic principles during comparisons of our experiments:

1) better performance on sparse noise test sets values more than that on intense noise test sets; and

2) higher sensitivity is more important than other metrics, especially specificity.

For the first point, if the future images are expected to have higher noise intensity due to, for instance, limitations of hardware, then models with better performance on intense noise images are preferred. The model selection is flexible and depends on the specific requirements. Here, we assume most of the future input images have sparse speckle noise.

According to the principles, best three models for each CNN in Stage I are selected after comprehensive comparisons as shown in Table 3 and 4. We use a check mark to note the model with the best performance in each metric. Specific performance numbers can not be provided here because it is a three-dimension data. For example, the sensitivity cell of AlexNet model *RtO* has six numbers behind: 82.84%, 78.03%, 74.89%, 70.8%, 66.42% and 65.31%. Each is the sensitivity value of the AlexNet *RtO* model on the original BUSI test set and its five noisy variant datasets. Therefore, we provide all the performance data in the GitHub repository.

Some models have a good performance in sensitivity while perform poorly in other metrics, such as *RtN_010_alexnet*, *RtN_008_resnet18* and *RtN_006_vgg16* on BUSI, and *RtN_010_alexnet*, *RtO_resnet18*, *RtN_008_resnet18*, *RtN_010_resnet50* and *RtN_006_vgg16* on MT_small. They are replaced by the one which has comparable sensitivity and much better performance in other metrics.

Table 3: Best model selections in Stage I based on their performance on BUSI test sets.

CNN	**Metric**	***RtO***	***RtN***					**Best Models**
			002	***004***	***006***	***008***	***010***	
AlexNet	**Sensitivity**		✓			✓	✓	RtN_002 RtN_008 RtN_010
	F1 score	✓	✓			✓		
	Accuracy		✓			✓	✓	
	Specificity	✓	✓		✓			
ResNet-18	**Sensitivity**			✓		✓	✓	RtO RtN_004 RtN_010
	F1 score			✓	✓		✓	
	Accuracy	✓		✓			✓	
	Specificity	✓		✓	✓			
ResNet-50	**Sensitivity**	✓	✓			✓		RtO RtN_002 RtN_008
	F1 score	✓	✓			✓		
	Accuracy	✓	✓			✓		
	Specificity		✓	✓	✓			
VGG16	**Sensitivity**	✓		✓	✓			RtO RtN_002 RtN_004
	F1 score	✓	✓	✓				
	Accuracy	✓	✓	✓				
	Specificity	✓	✓	✓				

5.3 Stage II

With the best models from Stage I, we construct training and validation sets by combining the corresponding Stage I training sets at certain mix proportions. Tuning the mix proportion depends on the behavior of Stage I models. The expectation of mix training is shown in Fig. 3, model A outperforms model B when noise intensity is low and otherwise when noise intensity is high. We would like to mix both training sets so that the new model obtains the most advantages of both model A and B, and achieve an ideal performance curve as model C. The bottom line of a mix-trained model is shown as model D, which has a mediocre performance compared to model A and B but demonstrates better capability of noise resilience. If a mix-trained model performs worse than this bottom line model, the mix-training is a failure and the corresponding mix proportion should be eliminated.

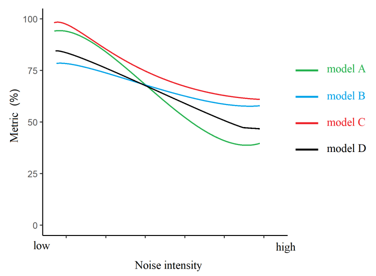

Figure 3: Mix-training Expectations.

In our experiment, mix proportion options are (20%, 40%, 40%), (25%, 50%, 25%), (33%, 33%, 33%) and (40%, 40%, 20%). Empirically, it is often the case that at least one of them generates a mix-trained model that has a close-to-optimal performance. We comprehensively compare four mix-trained models following the same rules and determine the best mix-trained model for each CNN. They are *mix_204040_alexnet*, *mix_404020_resnet18*, *mix_333333_resnet50* and *mix_404020_vgg16*. To show the mix-training performance gain, we compare them with the top three models in Stage I on BUSI and MT_small. The performance comparisons among the best three models in Stage I (*RtN_002*, *RtN_006*, *RtN_008*) and the best mix-trained model in Stage II (*mix_204040*) of AlexNet is provided in Table 5. The full performance numbers are available on GitHub. We plot the performance curves of all the best models in each stage for all CNNs in Fig. 4 and 5.

In all test scenarios, the mix-trained model has a more stable performance curve with limited fluctuation compared to single-trained models. One good example is *mix_204040_alexnet* on both test sets. It also achieves close-to-optimal performance curve on BUSI test sets as explained in Fig. 3. All VGG16 models share a stable and equally good performance in both test scenarios. However, *mix_333333_resnet50* performs worse than single-trained models in most scenarios on BUSI but has a decent performance on MT_small test sets. Therefore, all four mix proportions failed. On the other hand, *RtN_008_resnet50* champions in most test scenarios with a stable and good performance such as the sensitivity on each BUSI and MT_small test sets are {98.22%, 96.09%, 95.11%, 94.65%, 95.68%, 93.12%} and {99.22%, 96.86%, 96.75%, 97.96%,

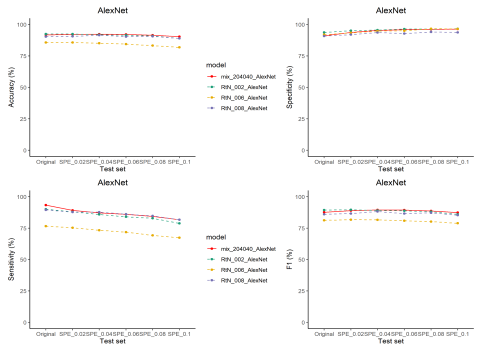

(a) AlexNet

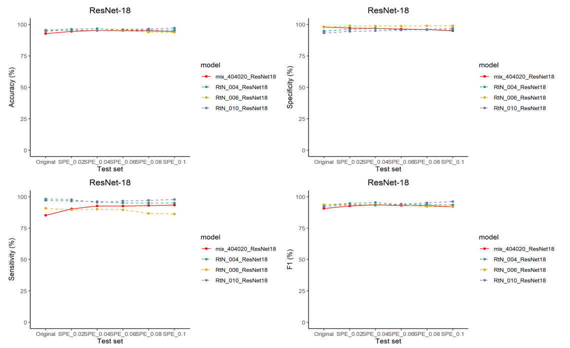

(b) ResNet-18

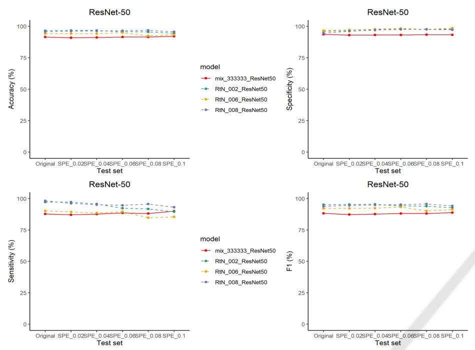

(c) ResNet-50

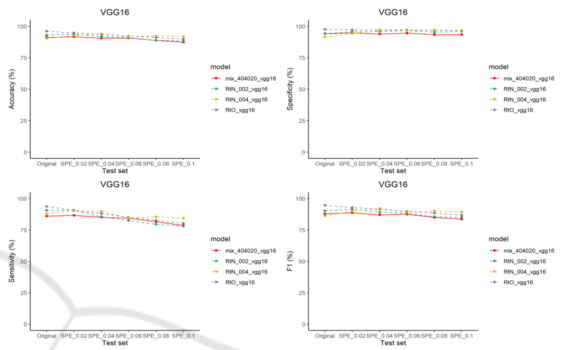

(d) VGG16

Figure 4: Best single-trained models (Stage I) vs. the best mix-trained model (Stage II) on BUSI.

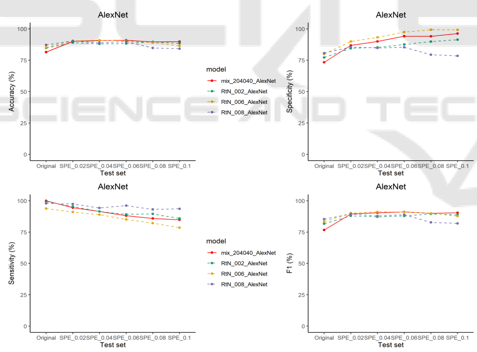

(a) AlexNet

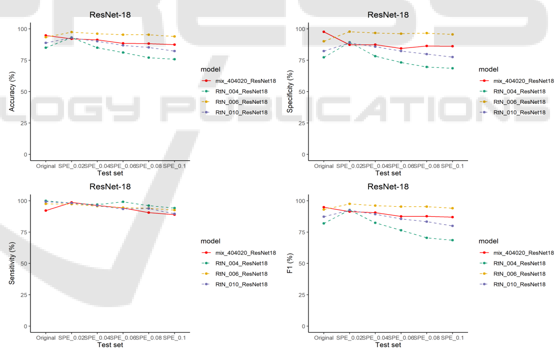

(b) ResNet-18

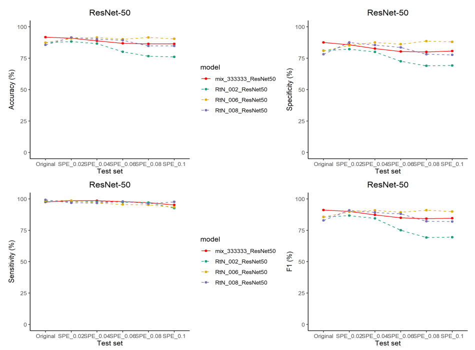

(c) ResNet-50

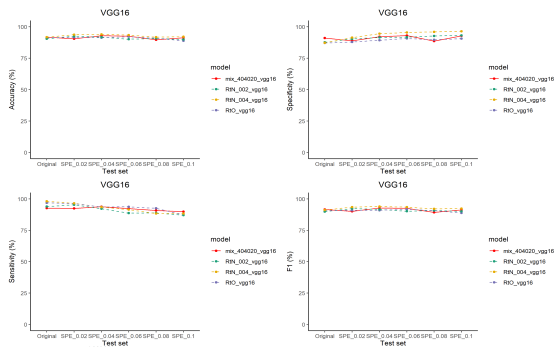

(d) VGG16

Figure 5: Best single-trained models (Stage I) vs. the best mix-trained model (Stage II) on MT_small.

Table 4: Best model selections in Stage I based on their performance on MT_small test sets.

CNN	Metric	*RtO*	*RtN*					Best Models
			002	***004***	***006***	***008***	***010***	
AlexNet	**Sensitivity**		✓			✓	✓	RtN_002 RtN_006 RtN_008
	F1 score	✓		✓	✓			
	Accuracy		✓		✓	✓		
	Specificity	✓		✓	✓			
ResNet-18	**Sensitivity**	✓				✓	✓	RtN_004 RtN_006 RtN_010
	F1 score		✓	✓			✓	
	Accuracy		✓	✓			✓	
	Specificity		✓	✓			✓	
ResNet-50	**Sensitivity**		✓			✓	✓	RtN_002 RtN_006 RtN_008
	F1 score			✓	✓	✓		
	Accuracy			✓	✓	✓		
	Specificity			✓	✓	✓		
VGG16	**Sensitivity**	✓		✓	✓			RtO RtN_002 RtN_004
	F1 score	✓	✓	✓				
	Accuracy	✓	✓	✓				
	Specificity		✓	✓			✓	

Table 5: The performance numbers of the best AlexNet models in each stage on original BUSI and its five noisy variant test sets: Under the metric cell, the six numbers in a row indicate the model's performance on *Original*, *SPE_002*, *SPE_004*, *SPE_006*, *SPE_008* and *SPE_010* variant of BUSI test set, respectively. The percent sign is omitted due to the width limit.

Model	Sensitivity						F1 score					
mix_204040	93.3	89.1	87.2	86.0	84.4	81.7	87.7	88.9	89.5	89.4	88.7	87.4
RtN_002	90.1	88.0	85.9	84.1	82.9	78.8	89.4	89.7	89.1	88.8	88.1	86.0
RtN_006	76.6	76.6	73.3	71.9	69.3	67.4	81.2	81.7	81.5	80.9	80.2	78.9
RtN_008	89.5	87.8	87.7	86.1	84.7	81.7	86.0	86.6	88.2	86.6	87.1	85.3
Model	**Accuracy**						**Specificity**					
mix_204040	91.8	92.1	92.3	92.1	91.6	90.4	91.0	93.8	95.4	96.0	96.2	96.4
RtN_002	92.5	92.5	92.0	91.6	91.0	89.1	93.8	95.1	95.7	96.5	96.5	96.7
RtN_006	85.8	85.8	85.2	84.5	83.3	82.0	92.0	93.4	94.8	95.1	96.6	96.5
RtN_008	90.4	90.6	91.6	90.4	90.6	89.1	90.9	92.1	93.7	92.8	94.2	93.7

96.27%, 97.69%}. It indicates that Stage II is sometimes redundant when one of the best models in Stage I achieves very decent performance. One abnormal phenomenon is the poor performance of single-trained ResNet-18 models on the Mt_small *Original* test set. Our explanation is that some random process in Stage I, such as random data sampling, costs the single-trained model missing benign nodule features.

In Table 6, we provide an empirical training scheme that generates a noise-trained model with the best performance for each backbone CNN.

Table 6: The training scheme for each backbone CNN: The training set is constructed by mixing the noise sets using the empirical proportion choice provided. For example, for AlexNet, the training set is developed by mixing *SPE*_002, *SPE*_006 and *SPE*_008 at a proportion of 20%, 40% and 40%. "000" in **Noise Set(s)** column indicates the original data without adding synthetic noise.

Backbone	Noise Set(s)	Mix Proportion
AlexNet	002,006,008	(20%, 40%, 40%)
ResNet-18	004,006,010	(40%, 40%, 20%)
ResNet-50	008	NA
VGG16	000,002,004	(40%, 40%, 20%)

6 CONCLUSIONS

In this study, we explore the impact of noisy data training on noisy data classification and propose a systematic two-stage noise training methodology. We mitigate the medical data shortage issue and overcome class imbalance problem by data augmentation and oversampling. We comprehensively compare the noise-trained models of three popular backbone CNNs in ultrasound image classification field and provide empirical training scheme for four tested CNNs. The conclusions regarding the proposed two-stage training methodology are as follows.

- The mix-trained model always has a more stable performance curve regardless the noise intensity. Thus, it is more resilient to speckle noise.
- The performance curve of a mix-trained model depends on the mix proportion of training sets corresponding to single-trained models in Stage I. A bad mix proportion choice may result in a disastrous performance curve.
- If a single-trained model in Stage I has an all-round decent performance, Stage II may be redundant, especially when other selected single-trained models perform much worse.

We are interested in flawed medical image processing such as breast ultrasound images with speckle noise because if enough information can be extracted from a low-quality medical image and useful conclusions can be developed, it would benefit more people with accessible and reliable medical advice. For future research, we plan to expand our work to other cancer types such as liver cancer, lung adenocarcinoma etc. Shortage of data is still the biggest challenge and we also plan to explore CNN architectures that generalize well on small training datasets.

ACKNOWLEDGEMENTS

The research reported in this paper is partially supported by the Philip and Virginia Sproul Professorship at Iowa State University and by the HPC@ISU equipment mostly purchased through funding provided by the NSF grants numbers MRI1726447 and MRI2018594.

REFERENCES

Al-Dhabyani, W., Gomaa, M., Khaled, H., and Fahmy, A. (2020). Dataset of breast ultrasound images. *Data in brief*, 28:104863.

Al-Haija, Q. A. and Adebanjo, A. (2020). Breast cancer diagnosis in histopathological images using resnet-50 convolutional neural network. In *2020 IEEE International IOT, Electronics and Mechatronics Conference (IEMTRONICS)*, pages 1–7. IEEE.

Albashish, D., Al-Sayyed, R., Abdullah, A., Ryalat, M. H., and Almansour, N. A. (2021). Deep cnn model based on vgg16 for breast cancer classification. In *2021 International Conference on Information Technology (ICIT)*, pages 805–810. IEEE.

Ayana, G., Park, J., Jeong, J.-W., and Choe, S.-w. (2022). A novel multistage transfer learning for ultrasound breast cancer image classification. *Diagnostics*, 12(1):135.

Badawy, S. M., Mohamed, A. E.-N. A., Hefnawy, A. A., Zidan, H. E., GadAllah, M. T., and El-Banby, G. M. (2021). Automatic semantic segmentation of breast tumors in ultrasound images based on combining fuzzy logic and deep learning—a feasibility study. *PloS one*, 16(5):e0251899.

Bhateja, V., Srivastava, A., Singh, G., and Singh, J. (2014). A modified speckle suppression algorithm for breast ultrasound images using directional filters. In *ICT and Critical Infrastructure: Proceedings of the 48th Annual Convention of Computer Society of India-Vol II*, pages 219–226. Springer.

Buda, M., Maki, A., and Mazurowski, M. A. (2018). A systematic study of the class imbalance problem in convolutional neural networks. *Neural networks*, 106:249–259.

Chang, Y., Yan, L., Chen, M., Fang, H., and Zhong, S. (2019). Two-stage convolutional neural network for medical noise removal via image decomposition. *IEEE Transactions on Instrumentation and Measurement*, 69(6):2707–2721.

Daoud, M. I., Abdel-Rahman, S., and Alazrai, R. (2019). Breast ultrasound image classification using a pre-trained convolutional neural network. In *2019 15th International Conference on Signal-Image Technology & Internet-Based Systems (SITIS)*, pages 167–171. IEEE.

Deng, J., Dong, W., Socher, R., Li, L.-J., Li, K., and Fei-Fei, L. (2009). Imagenet: A large-scale hierarchical image database. In *2009 IEEE conference on computer vision and pattern recognition*, pages 248–255. Ieee.

Dodge, S. and Karam, L. (2016). Understanding how image quality affects deep neural networks. In *2016 eighth international conference on quality of multimedia experience (QoMEX)*, pages 1–6. IEEE.

Forouzanfar, M. and Abrishami-Moghaddam, H. (2011). Ultrasound speckle reduction in the complex wavelet domain.

Hadad, O., Bakalo, R., Ben-Ari, R., Hashoul, S., and Amit, G. (2017). Classification of breast lesions using cross-modal deep learning. In *2017 IEEE 14th International Symposium on Biomedical Imaging (ISBI 2017)*, pages 109–112. IEEE.

He, K., Zhang, X., Ren, S., and Sun, J. (2016). Deep residual learning for image recognition. In *Proceedings of* *the IEEE conference on computer vision and pattern recognition*, pages 770–778.

Jahangeer, G. S. B. and Rajkumar, T. D. (2021). Early detection of breast cancer using hybrid of series network and vgg-16. *Multimedia Tools and Applications*, 80(5):7853–7886.

Jiang, Y., Chen, L., Zhang, H., and Xiao, X. (2019). Breast cancer histopathological image classification using convolutional neural networks with small se-resnet module. *PloS one*, 14(3):e0214587.

Kim, H. E., Cosa-Linan, A., Santhanam, N., Jannesari, M., Maros, M. E., and Ganslandt, T. (2022). Transfer learning for medical image classification: a literature review. *BMC medical imaging*, 22(1):1–13.

Krizhevsky, A., Sutskever, I., and Hinton, G. E. (2012). Imagenet classification with deep convolutional neural networks. *Advances in neural information processing systems*, 25.

LeCun, Y., Bengio, Y., and Hinton, G. (2015). Deep learning. *nature*, 521(7553):436–444.

Li, X., Wang, Y., Zhao, Y., and Wei, Y. (2022). Fast speckle noise suppression algorithm in breast ultrasound image using three-dimensional deep learning. *Frontiers in Physiology*, page 698.

Ling, C. X. and Li, C. (1998). Data mining for direct marketing: Problems and solutions. In *Kdd*, volume 98, pages 73–79.

Liu, S., Wang, Y., Yang, X., Lei, B., Liu, L., Li, S. X., Ni, D., and Wang, T. (2019). Deep learning in medical ultrasound analysis: a review. *Engineering*, 5(2):261–275.

Masud, M., Hossain, M. S., Alhumyani, H., Alshamrani, S. S., Cheikhrouhou, O., Ibrahim, S., Muhammad, G., Rashed, A. E. E., and Gupta, B. (2021). Pre-trained convolutional neural networks for breast cancer detection using ultrasound images. *ACM Transactions on Internet Technology (TOIT)*, 21(4):1–17.

Moon, W. K., Lee, Y.-W., Ke, H.-H., Lee, S. H., Huang, C.-S., and Chang, R.-F. (2020). Computer-aided diagnosis of breast ultrasound images using ensemble learning from convolutional neural networks. *Computer methods and programs in biomedicine*, 190:105361.

Nawaz, W., Ahmed, S., Tahir, A., and Khan, H. A. (2018). Classification of breast cancer histology images using alexnet. In *International conference image analysis and recognition*, pages 869–876. Springer.

Russakovsky, O., Deng, J., Su, H., Krause, J., Satheesh, S., Ma, S., Huang, Z., Karpathy, A., Khosla, A., Bernstein, M., et al. (2015). Imagenet large scale visual recognition challenge. *International journal of computer vision*, 115(3):211–252.

Sarvamangala, D. and Kulkarni, R. V. (2021). Convolutional neural networks in medical image understanding: a survey. *Evolutionary intelligence*, pages 1–22.

Simonyan, K. and Zisserman, A. (2014). Very deep convolutional networks for large-scale image recognition. *arXiv preprint arXiv:1409.1556*.

Taha, A. A. and Hanbury, A. (2015). Metrics for evaluating 3d medical image segmentation: analysis, selection, and tool. *BMC medical imaging*, 15(1):1–28.

Virmani, J., Agarwal, R., et al. (2019). Assessment of despeckle filtering algorithms for segmentation of breast tumours from ultrasound images. *Biocybernetics and Biomedical Engineering*, 39(1):100–121.

Virmani, J., Agarwal, R., et al. (2020). Deep feature extraction and classification of breast ultrasound images. *Multimedia Tools and Applications*, 79(37):27257–27292.

Wang, Y., Ge, X., Ma, H., Qi, S., Zhang, G., and Yao, Y. (2021). Deep learning in medical ultrasound image analysis: a review. *IEEE Access*, 9:54310–54324.

Yap, M. H., Goyal, M., Osman, F., Martí, R., Denton, E., Juette, A., and Zwiggelaar, R. (2020). Breast ultrasound region of interest detection and lesion localisation. *Artificial Intelligence in Medicine*, 107:101880.

Yu, X., Kang, C., Guttery, D. S., Kadry, S., Chen, Y., and Zhang, Y.-D. (2020). Resnet-scda-50 for breast abnormality classification. *IEEE/ACM transactions on computational biology and bioinformatics*, 18(1):94–102.

Yuan, L., Chen, D., Chen, Y.-L., Codella, N., Dai, X., Gao, J., Hu, H., Huang, X., Li, B., Li, C., et al. (2021). Florence: A new foundation model for computer vision. *arXiv preprint arXiv:2111.11432*.